ACS OMEGA

http://pubs.acs.org/journal/acsodf

Article

Systematic Development of Solid Lipid Nanoparticles of Abiraterone Acetate with Improved Oral Bioavailability and Anticancer Activity for Prostate Carcinoma Treatment

Sarwar Beg,*[,] Ankit K. Malik,[] Mohammad Javed Ansari,* Asrar A. Malik, Ahmed Mahmoud Abdelhaleem Ali, Abdulrahman Theyab, Mohammad Algahtani, Waleed H. Almalki, Khalid S. Alharbi, Sattam K. Alenezi, Md. Abul Barkat, Mahfoozur Rahman, and Hani Choudhry

Cite This: *ACS Omega* 2022, 7, 16968−16979

Read Online

ACCESS | Metrics & More | Article Recommendations | Supporting Information

ABSTRACT: In the present work, an attempt was undertaken to improve the oral bioavailability and anticancer activity of abiraterone acetate. Solid lipid nanoparticles (SLNs) were developed using the quality by design (QbD) principles and evaluated through *in vitro*, *ex vivo*, and *in vivo* studies. Solid lipid suitability was evaluated by equilibrium solubility study, while surfactant and cosurfactant were screened based on the ability to form microemulsion with the selected lipid. SLNs were prepared by emulsion/solvent evaporation method using glyceryl monostearate, Tween 80, and Poloxamer 407 as the solid lipid, surfactant, and cosurfactant, respectively. Box-Behnken design was applied for optimization of material attributes and evaluating their impact on particle size, polydispersity index, zeta potential, and entrapment efficiency of the SLNs. *In vitro* drug release study was evaluated in simulated gastric and intestinal fluids. Cell culture studies on PC-3 cells were performed to evaluate the cytotoxicity of the drug-loaded SLNs in comparison to the free drug suspension. Qualitative uptake was evaluated for Rhodamine B-loaded SLNs and compared with free dye solution. *Ex vivo* permeability was evaluated on Wistar rat intestine and *in vivo* pharmacokinetic evaluation on Wistar rats for SLNs and free drug suspension. Concisely, the SLNs showed potential for significant improvement in the biopharmaceutical performance of the selected drug candidate over the existing formulations of abiraterone acetate.

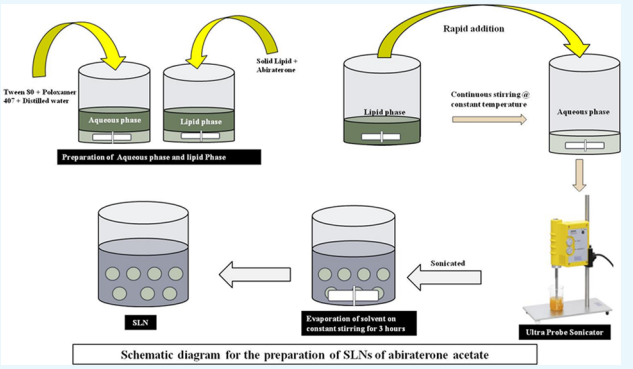

1. INTRODUCTION

Prostate carcinoma is the second-leading cause of death worldwide after breast cancer. As per the global cancer statistics 2020, prostate carcinoma accounted for nearly 375 000 deaths across the globe, while around 1 414 259 new cases were reported in the same year.[1] In the U.S., 1 in 9 men is diagnosed with prostate carcinoma. Within the population affected with prostate carcinoma, nearly 10−15% of the cases belong to metastatic castration-resistant and high-risk castration-sensitive prostate carcinomas.[2] Hence, these are considered as the deadliest neoplasms and one of the worst prognosis variants. The castration-resistant prostate carcinoma occurs in males undergoing androgen depletion therapy and continues to rise with the depletion of levels of serum prostate-specific antigen, which also leads to new metastases. In the majority of the population, the early diagnosis can offer a better prognosis to prostate carcinoma patients.[3]

Although surgical and chemical castration methods are used under the standard treatment, over 85% of cancer patients exhibit metastasis.[4] Literature reports have demonstrated the use of docetaxel for the treatment of aggressive castration-resistant prostate carcinoma with a 20% improvement in the median survival rate. However, docetaxel therapy also faces challenges with drug resistance, and it only provides symptomatic relief.[5] In this regard, abiraterone acetate is recommended as the alternative drug therapy over docetaxel for the treatment of castration-resistant prostate carcinoma.[6]

Abiraterone acetate, a prodrug approved by USFDA in 2011, is used especially for the treatment of metastatic castration-resistant and high-risk castration-sensitive prostate carcinoma in combination with corticosteroids like prednisolone.[7] Chemically, abiraterone is a steroidal progesterone derivative, which is present in the form of 3-O-acetyl abiraterone. The

Received: December 23, 2021
Accepted: March 3, 2022
Published: May 10, 2022

presence of plasma esterases in the body helps in the conversion of abiraterone acetate to its active form abiraterone by deacetylation process after oral administration.[8] It acts by reducing the synthesis of androgens by inhibiting the CYP17A1 isozyme responsible for the production of testosterone and its effect on prostate carcinoma cells.[9] Despite the very good therapeutic potential, abiraterone acetate classified under BCS class IV, exhibit biopharmaceutical challenges like polymorphism, poor solubility (<0.5 μg/mL), high lipophilicity (LogP 5.12) and inconsistent permeability, and low oral bioavailability (<10%) along with the presence of positive food-effect.[10] This often requires a high dose (1000 mg daily) to attain the required therapeutic effects of the drug.

The development of novel drug delivery systems for an existing drug molecule, instead of designing new drugs, can overcome the challenges with novel drug therapy. There are only a few research studies in the literature about the novel formulations of abiraterone. As per the literature analysis, the published reports have focused primarily on the stabilization of polymorphic forms of the drug.[11] A few reports have been published about the solid dispersions and silica lipid hybrid nanoparticles of abiraterone acetate.[12] Although these studies have addressed some of the drug delivery challenges of abiraterone, the manufacturing methods are difficult to reproduce. Hence, the described work endeavored to design a robust nanoparticle formulation of abiraterone for oral bioavailability improvement.

Solid lipid nanoparticles (SLNs) are the most promising alternatives because of the ease of preparation and excellent formulation stability. These are prepared using biocompatible lipids and are very popular for their immense ability for delivering highly lipophilic drugs.[13,14] SLNs possess various advantages over polymeric nanoparticles like high drug loading capacity, surface functionalization ability, ease of manufacturing, and scale-up characteristics.[15,16] Lipid nanoparticles are reported to be suitable for the stabilization of pharmaceuticals, exhibiting polymorphism problems. A variety of options are available in lipid selection for designing SLNs capable of addressing the drug delivery challenges. One of the extensively investigated applications of SLNs include oral drug bioavailability improvement.[17,18]

For the selected drug candidate, abiraterone acetate, SLNs were prepared from the biomimetic lipids to improve the oral bioavailability and anticancer activity against prostate carcinoma cells. The lipid nanoparticles attempted to overcome the biopharmaceutical challenges of abiraterone acetate followed by selective absorption of the drug through the oral route, thus improving the anticancer activity.[19] Further, surface functionalization of SLNs with ligands, peptides, antigens, and so forth also helps them in achieving tumor-specific drug targeting. For attaining the best therapeutic performance, systematic optimization of the nanopharmaceutical drug products is essential.[20] In this regard, the implementation of quality by design (QbD) principles in drug product optimization provides the best optimal solution.[2122] Besides,[23] QbD also[24] facilitates product[25] and process understanding, as it applies science and risk-based principles to identify the influential factors, optimizing them. Several research studies have documented the role of QbD approach in the development of nanoparticle formulations, which provides enormous flexibility postoptimization during scale-up variation.

The current research work, therefore, discussed the development of SLNs-loaded with abiraterone acetate and Rhodamine B for the evaluation of improvements in oral bioavailability and anticancer activity on prostate carcinoma cells. The prepared nanoparticles were subjected to thorough characterization with the help of *in vitro* and *in vivo* studies for evaluating their worth in augmenting the anticancer activity of the drug.

2. RESULTS AND DISCUSSION

2.1. Screening of Lipids. The selection of solid lipid was done on the basis of the evaluation of the maximum solubility of the drug in different lipids. Figure 1 illustrates the equilibrium solubility data of abiraterone acetate in various solid lipids where maximum solubility of the drug was observed in glyceryl monostearate (0.062 mg/kg of lipid) and minimum solubility was observed in Labrafil M1944 (0.009 mg/kg of lipid). Higher solubility in glyceryl monostearate could be attributed to the presence of long-chain triglycerides, thus considered as very appropriate for the preparation of SLNs.[13,16,26]

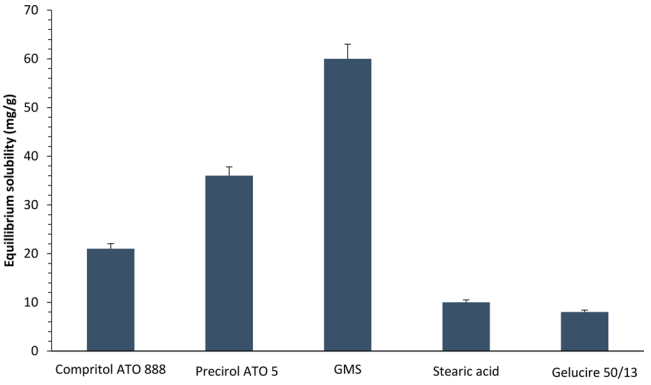

Figure 1. Equilibrium solubility data of abiraterone acetate in various lipids; data expressed as mean ± SD (n = 3). GMS: glyceryl monostearate.

2.2. Screening of Surfactant and Cosurfactant. The selection of surfactant and cosurfactant was made by performing screening studies by preparing trial SLN formulations to evaluate percent transmittance as a parameter to evaluate phase clarity of the formulation. Figure 2 illustrates

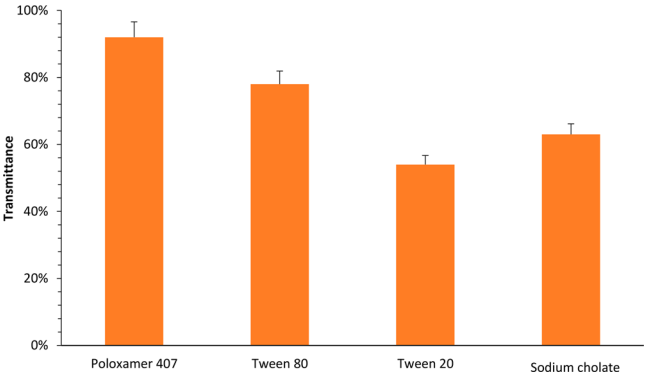

Figure 2. Percentage transmittance of surfactants studied in combination with lipids having maximal drug solubility; data expressed as mean ± SD (n = 3).

https://doi.org/10.1021/acsomega.1c07254
ACS Omega 2022, 7, 16968−16979

Table 1. Design Matrix as per Box-Behnken Design Used for Optimization of the SLNs of Abiraterone Acetate[a]

trials	Factor A: concentration of GMS (mg)	Factor B: concentration of Tween 80 (%)	Factor C: concentration of Poloxamer 407 (%)	Response 1 Y1: particle size (nm)	Response 2 Y2: polydispersity index	Response 3 Y3: entrapment efficiency (%)
11	50	3	2	375	0.301	80
7	40	4	2	197	0.233	76
8	60	4	2	529	0.295	85
12	50	5	2	289	0.225	74
1	40	3	1.5	224	0.283	65
4	60	5	1.5	529	0.295	85
14	50	4	1.5	299	0.425	70
13	50	4	1.5	299	0.425	70
15	50	4	1.5	299	0.425	70
2	60	3	1.5	560	0.301	80
3	40	5	1.5	185	0.205	68
9	50	3	1	360	0.301	80
6	60	4	1	613	0.319	77
5	40	4	1	204	0.283	65
10	50	5	1	560	0.301	80

[a]All formulations were prepared in triplicate. Data expressed as mean ± SD (n = 3).

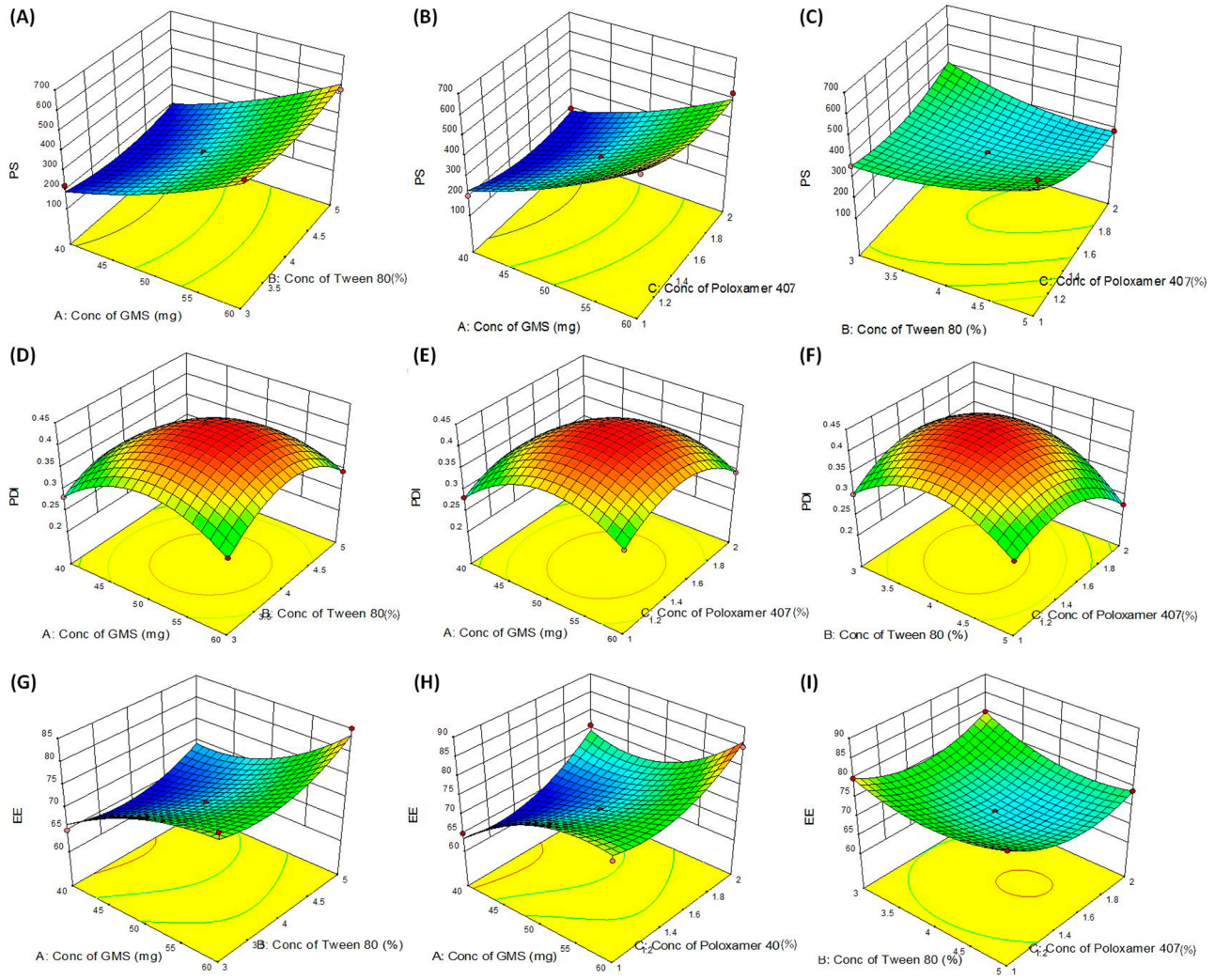

Figure 3. Response surface plots depicting the impact of factors (A) conc. of GMS and Tween 80, (B) conc. of GMS and Poloxamer 407, (C) conc. of Tween 80 and Poloxamer 407 on particle size, (D) conc. of GMS and Tween 80, (E) conc. of GMS and Poloxamer 407, (F) conc. of Tween 80 and Poloxamer 407 polydispersity index and (G) conc. of GMS and Tween 80, (H) conc. of GMS and Poloxamer 407, (I) conc. of Tween 80 and Poloxamer 407 entrapment efficiency as the response variables.

https://doi.org/10.1021/acsomega.1c07254
ACS Omega 2022, 7, 16968−16979

the percent transmittance observed for various surfactants and cosurfactant, where Poloxamer 407 and Tween 80 showed 92% and 78% transmittance for the investigated trial SLN formulations. A high transmittance is an indicator of the nanosized particle dimension and stable nature of the prepared formulation, hence both Poloxamer 407 and Tween 80 were selected further for optimization studies.[15,27]

2.3. Systematic Optimization of SLNs Using Experimental Design. As per the systematic approach adopted for formulation development, the impact of selected material attributes was evaluated on the response variables. Table 1 enlists the values of response variables obtained for the formulations as per the BBD. Further, mathematical modelization of the data indicated best fitting to a quadratic polynomial equation for all the responses. The quadratic model was constituted of linear and quadratic interaction terms with all the statistical parameters (i.e., correlation coefficient close to 1, predicted error close to 0, and model p-values <0.05) within the acceptance range. Supporting Information Tables S1−S3 provide detailed data on mathematical model fitting employed for the response variables along with the statistical parameters. With the best-fitted models, 3D- and 2D-response surface plots were analyzed for studying the impact of factors on the responses. Figure 3 illustrates 3D- and 2D-response surface graphs for various particle size, polydispersity index, and entrapment efficiency as the response variables.

From the graphs in Figure 3A−C depicting the effect of studied factors on particle size, it can be clear that the effect of concentration of lipid (GMS) was more prominent while surfactants (Tween 80 and poloxamer 407) showed only mild influence. Smaller particle size was observed at low concentration of lipid and high concentration of surfactants and vice versa. As lipid (GMS) exhibits a vital role in controlling the matrix structure of the SLNs, high lipid concentrations yielded larger particles.[13,26] On the contrary, the concentration of surfactant (Tween 80) helped in reducing the particle size due to its surface tension lowering property. Moreover, stabilizer concentration (Poloxamer 407) exhibited only mild positive influence in reducing the particle size thus was added in low concentration for attaining good thermodynamic stability of the SLNs. Like particle size, the 3D- and 2D-response surface plots depicted in Figure 3D−F for polydispersity index also showed analogous relationships among the studied factors on the response variables. The analysis of the effect of factors on the response variable entrapment efficiency was studied using 3D- and 2D-response surface plots asshown in Figure 3G−I. The high entrapment efficiency of the drug was observed in SLNs at higher lipid and surfactant concentrations while at an intermediate concentration of the stabilizer. Because of the low impact of stabilizer concentration on the drug entrapment with a high impact of lipid and surfactant concentrations, the target ranges of response variables were provided to select the optimized formulation by numerical and graphical search methods.

2.4. Selection of the Optimized SLNs and Validation Results. The numerical and graphical search method for selecting the optimized SLNs was provided with the target range of particle size between 100 to 250 nm, polydispersity index between 0.1 to 0.3, and entrapment efficiency between 70 to 90%. The optimized SLN formula was selected by numerical optimization desirability function close to 1 as such optimum formulation shows a high degree of predictability. Table 2 enlists the optimum formula of weight quantities of the

Table 2. Results of Numeric Optimization for SLNs of Abiraterone Acetate[a]

variable	goal	lower limit	upper limit
Critical Material Attributes			
A: concentration of GMS (mg)	in range	40	60
B: concentration of Tween 80 (%)	in range	3	5
C: concentration of Poloxamer 407 (mg)	in range	1	2
Critical Quality Attributes			
Y1: particle size (nm)	in range	100	250
Y2: polydispersity index	in range	0.1	0.3
Y3: Entrapment efficiency (%)	in range	70%	90%

predicted solutions						
A	B	C	PS	PDI	EE	desirability value
44.9	4.5	1.8	209.3	0.28	70.1	1.00
42.8	3.8	1.8	204.4	0.31	70.5	1.00
46.0	4.6	1.8	223.5	0.28	70.3	1.00

[a]PS, particle size; PDI, polydispersity index; EE, entrapment efficiency.

lipid, surfactant, and stabilizer concentration in the SLNs with the predicted values of the responses variables. The optimized formulation was constituted of concentration of lipid (GMS) at 50 mg, concentration of surfactant (Tween 80) at 4%, and concentration of stabilizer (Poloxamer 407) at 1.5%, which exhibited predicted values of particle size of 181 nm, polydispersity index of 0.247, and entrapment efficiency of 97%.

The chosen optimized formulation was further checked for spatial location in the overlay plot by graphical search method, which was found to be well within the design space region as shown in Figure 4. The validation exercise was performed by comparing predicted and actual values of the responses, as shown in Supporting Information Table S4. The results revealed percent prediction error was within ±10% for all the responses and construed good predictability of the selected mathematical model.

2.5. Characterization of the Optimized SLNs. *2.5.1. Particle Size and Zeta Potential.* The optimized drug-loaded SLNs exhibited particles of 197.2 nm when measured using dynamic light scattering as shown in Figure 5A, which indicated the nanostructured nature of the prepared SLNs. Further, the polydispersity index was found to be 0.216 with a single sharp peak also construed the monodisperse nature of the particles in SLNs. The rational selection of excipients and their concentrations was helpful in selecting the SLNs with smaller particle size and good polydispersity index.[13,26] Figure 5B revealed the zeta potential value of 110 mV for the optimized SLNs measured using photon correlation spectroscopy, which indicated the stable nature of the optimized SLN formulation. It is quite usual that nanoparticles with zeta potential between −30 and 30 mV demonstrate good colloidal stability for longer periods of time.[28−30] However,[30] the SLNs of abiraterone[29] acetate prepared in the current work showed very high zeta potential which could be attributed to the presence of lipids and emulgents selected for the preparation of the SLNs.

2.5.2. Entrapment Efficiency. The optimized drug-loaded SLNs exhibited good entrapment efficiency of 77% for abiraterone acetate, which was well within the level of acceptance for the selection of optimum formulation. High

https://doi.org/10.1021/acsomega.1c07254
ACS Omega 2022, 7, 16968−16979

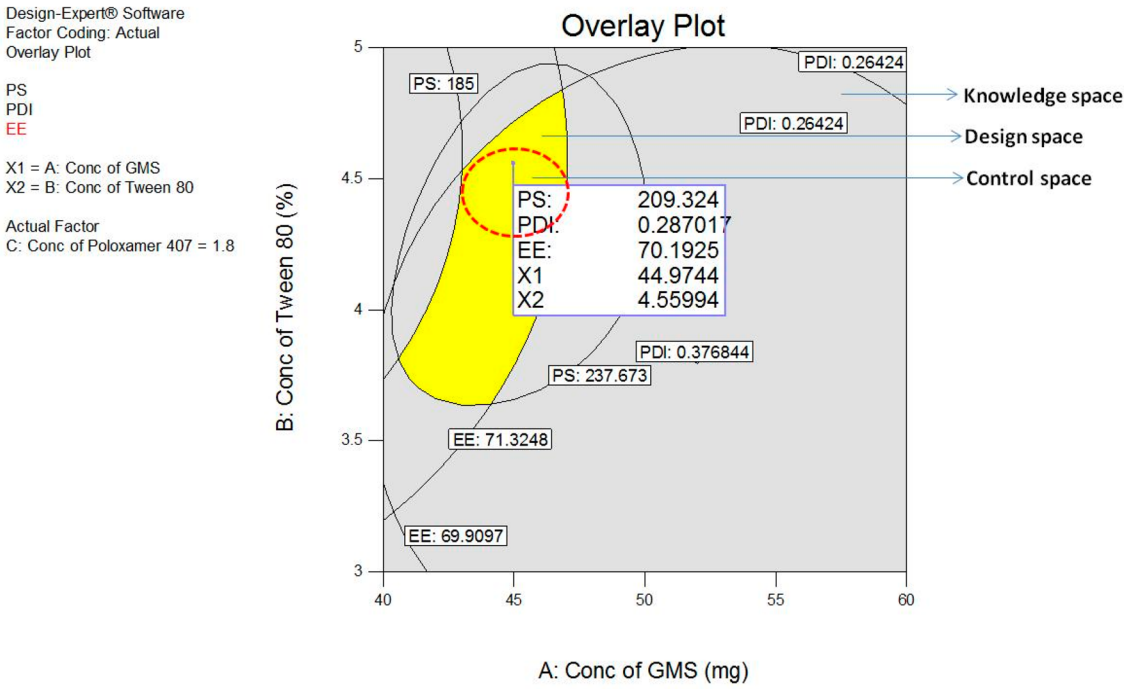

Figure 4. Design space overlay plot depicting the composition of optimized SLNs formulation and predicted values of the response variables.

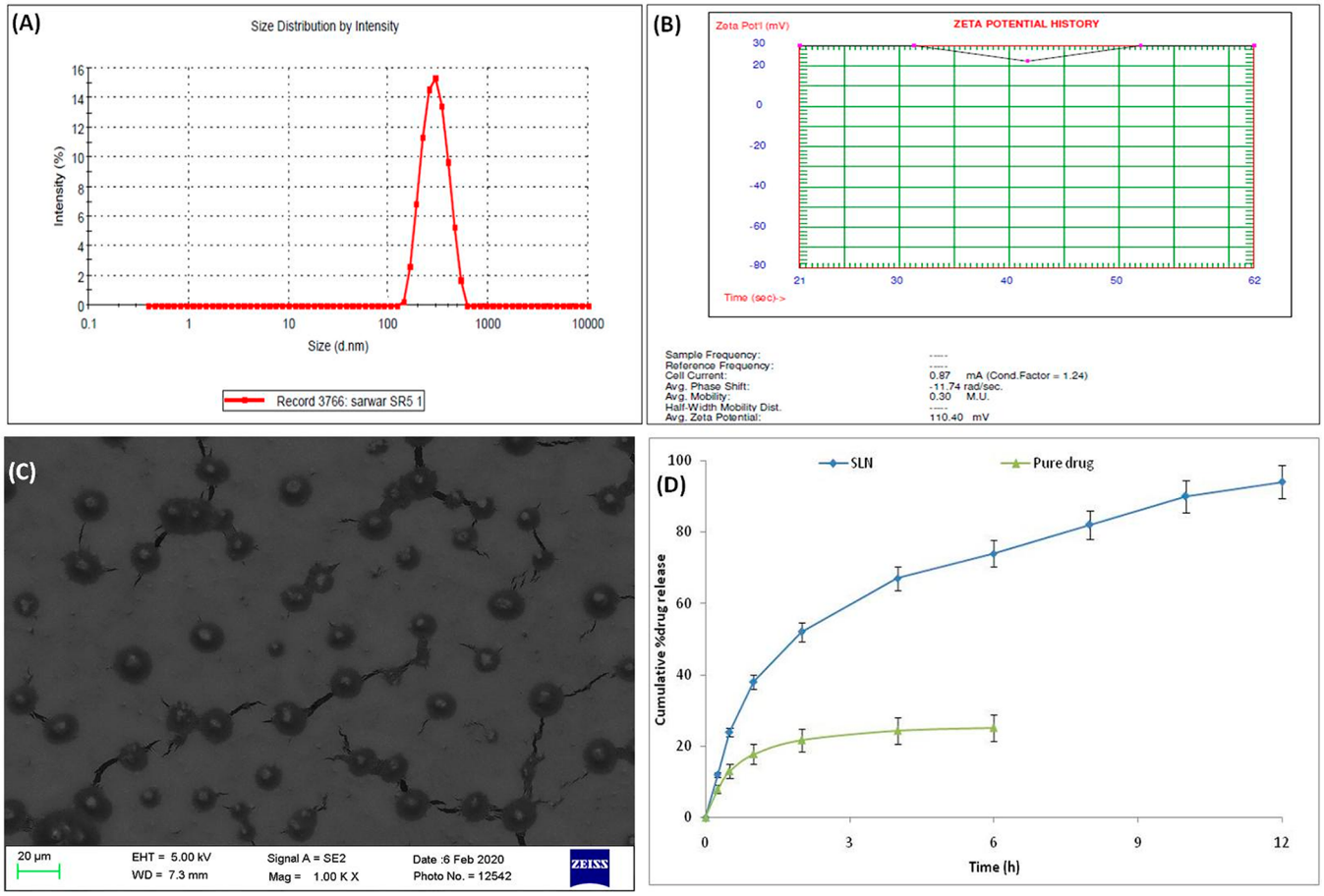

Figure 5. (A) Particle size distribution, (B) zeta potential distribution, (C) scanning electron microscopy image, and (D) *in vitro* drug release profiles of the optimized SLNs of abiraterone acetate where data expressed as mean ± SD (n = 3).

drug entrapment efficiency is desirable for getting maximal therapeutic efficacy, and it endeavored for the optimized SLNs prepared in the present work.[16,31] From the systematic optimization approach, the best lipid and surfactant concen-

https://doi.org/10.1021/acsomega.1c07254
ACS Omega 2022, 7, 16968−16979

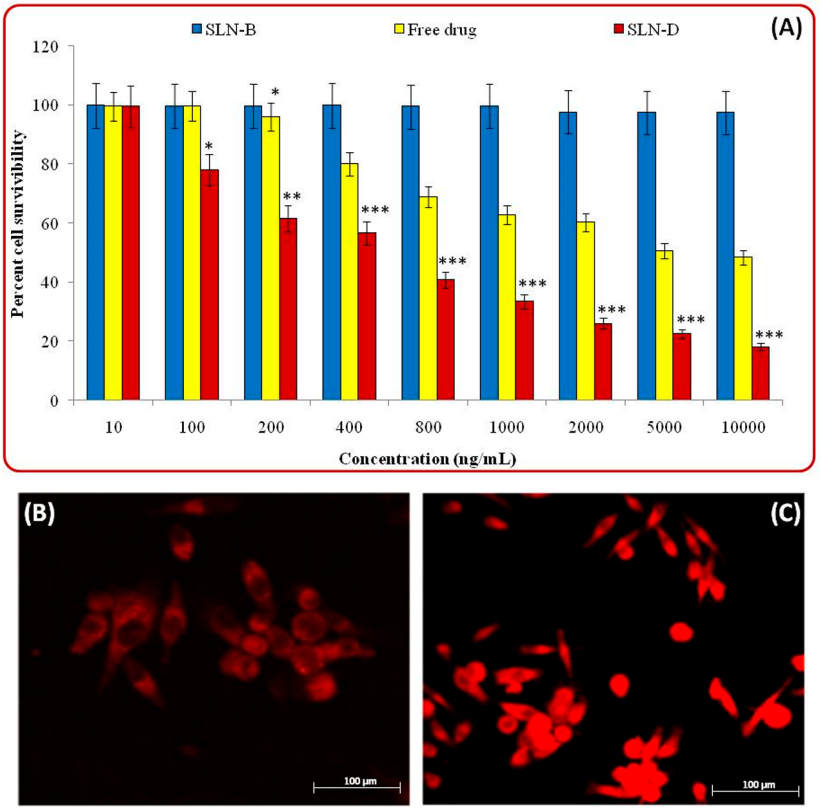

Figure 6. (A) Cytotoxicity analysis by MTT assay, data expressed as mean ± SD (n = 3). (B,C) Confocal laser scanning microscopy images of the uptake of plain Rhodamine B and SLNs loaded with Rhodamine B dye. SLN-B, blank SLNs; SLN-D, drug-loaded SLNs.

tration yielding maximal entrapment efficiency was selected. For highly lipophilic drugs, lipid-based nanocarriers have proven to be quite effective to provide high drug entrapment efficiency which was also observed in the current work for the developed nanoparticles.

2.5.3. Scanning Electron Microscopy (SEM). The bright-field SEM images of optimized drug-loaded SLNs showed nanoparticles with the spherical shape in visual appearance under 100× magnification. Figure 5C illustrates the surface morphology of SLNs with the spherical appearance of the particles with size ranging between 170 to 177 nm which was found to be quite analogous to the particle size by dynamic light scattering method. The uniformity in size and globular structure of the particles is helpful for permeation through biological barriers into the systemic circulation.[14,17]

2.5.4. In Vitro Drug Release Studies. The *in vitro* release profiles of abiraterone acetate from the optimized SLNs and pure drug suspension in 0.1 N HCl (pH 1.2) for 2 h and phosphate buffer solution (pH 6.8) for 24 h are shown in Figure 5D. From SLNs, the drug release profile was found to be quite sustained and nearly complete drug release was observed within the studied time period. On the contrary, pure drug suspension showed only 24% drug release in the medium within the initial 2 h, followed by a plateau phase indicating no further change in drug release profile. Statistical data analysis indicated a highly significant difference in the percent drug release at all the studied time points ($p < 0.05$). The enhanced release profile of the drug from SLNs could be ascribed to its lipophilic characteristic which helped in maximal drug entrapment followed by micellar solubilization of abiraterone acetate. However, an incomplete release observed from the pure drug suspension is attributed to its poor aqueous solubility characteristics, as clearly evident from the drug release graph and discussed in literature reports.[32,33]

2.5.5. In Vitro Cell Culture Studies. 2.5.5.1. Cell Cytotoxicity Assay. The cellular cytotoxicity was performed by MTT assay to evaluate the cell viability (PC-3) from the optimized SLNs of abiraterone acetate loaded with Rhodamine B and plain Rhodamine B dye solution. The cell viability data shown in Figure 6A reveals that SLNs showed IC_{50} value at concentration 400 ng/mL, while free drug suspension showed an IC_{50} value at 5000 ng/mL ($p < 0.001$). Nearly 12.5-fold reduction in IC_{50} value of the drug abiraterone was observed from SLNs indicated higher efficacy of SLNs on castration-resistant PC-3 prostate carcinoma cells. This could be attributed to the enhanced permeability, uptake, and retention of SLNs in the cancer cells to exhibit a high degree of cytotoxic activity for reducing the survival of the cells.[13,15,16]

2.5.5.2. Cell Uptake Study. The cell uptake study was performed to visually evaluate the uptake performance of treatment groups on PC-3 cells. As illustrated in Figure 6B,C, SLNs tagged with Rhodamine B were subjected to CLSM imaging showed higher uptake over the plain dye solution within an incubation period of 4 h. The percent fluorescence intensity was higher with SLNs, which revealed the suitability of the SLNs as a promising carrier system to encapsulate and deliver the drug to the cells. During this study, different batches of SLNs were prepared by adding Rhodamine B to the aqueous and/or lipidic phase during formulation. SLNs with the dye added to the lipidic phase exhibited high fluorescence intensity as compared to the dye added to the aqueous phase. This could be ascribed to the higher affinity of Rhodamine B to the lipid phase which might have been responsible for uptake of the SLNs into the PC-3 cells.[31,34] Besides, dye concentration

https://doi.org/10.1021/acsomega.1c07254
ACS Omega 2022, 7, 16968−16979

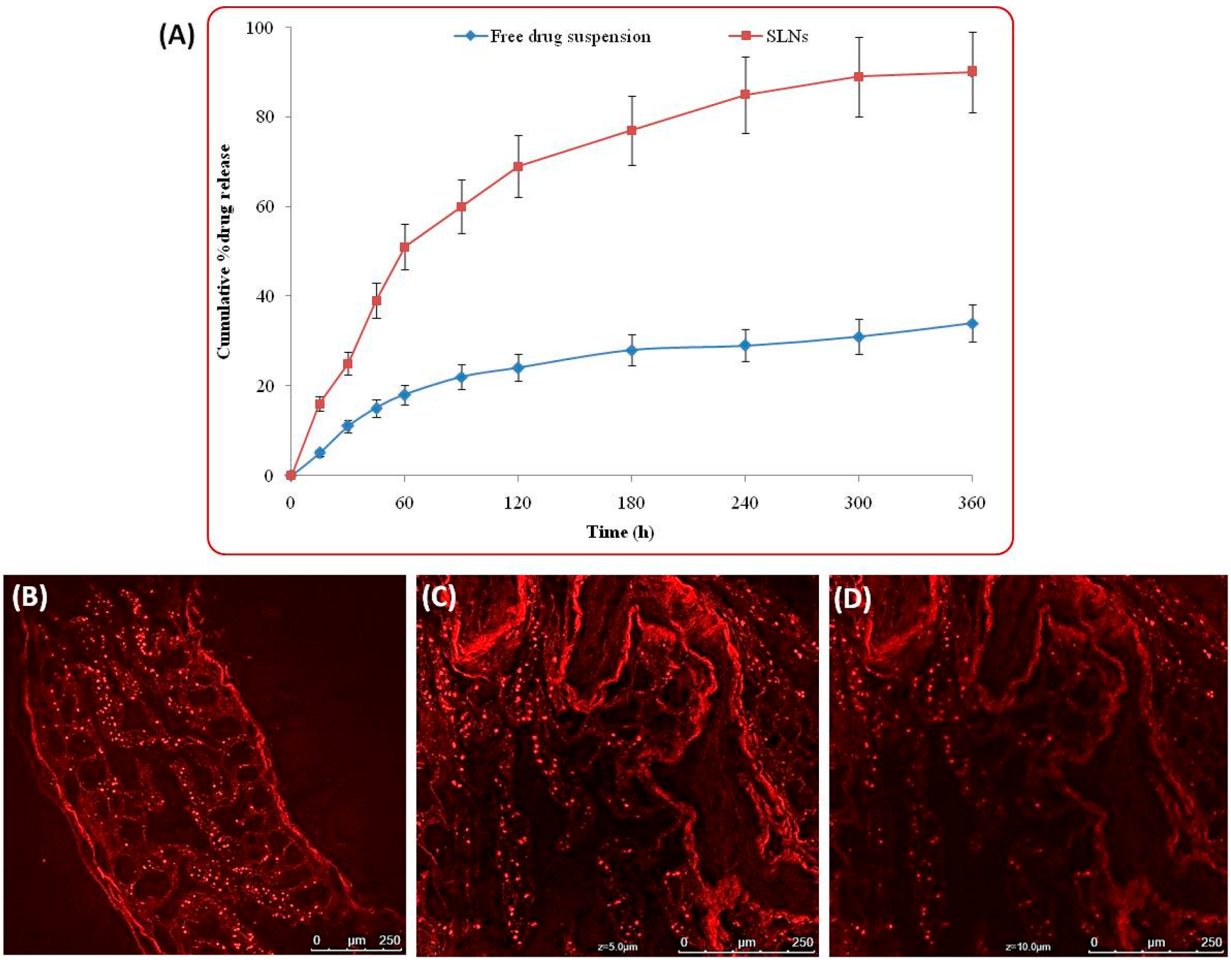

Figure 7. (A) *Ex vivo* permeation data of abiraterone acetate from SLNs and free drug suspension, data expressed as mean ± SD (n = 3). (B) Confocal laser scanning microscopy images of the uptake of Rhodamine B loaded SLNs at 100× magnification while (C,D) showed z-stacking performed for measurement of permeation of SLNs up to 5 and 10 μm depth in the intestinal tissue segments.

in the formulation was also investigated which revealed that best results were observed at 1 μg/mL of Rhodamine B in all cases, whereas at the same concentration of free Rhodamine B the fluorescence intensity was found to be very weak. The cell culture studies revealed excellent cytotoxicity and uptake potential of the SLNs of abiraterone acetate on PC-3 cancer cells.

2.5.6. Ex Vivo Permeation and Confocal Microscopy Imaging. *Ex vivo* permeation studies were performed using rat intestine on the duodenum and jejunum sections, which revealed percent permeation of drug from the optimized SLNs of abiraterone acetate and pure drug suspension. Figure 7A illustrates the graph showing cumulative percent drug permeated through different parts of the small intestine. The permeation of drug from SLNs was found to be quite higher (3.75-fold; $p < 0.05$) as compared to the pure drug suspension which indicated superior permeability potential of the drug delivered through SLNs. Further, confocal microscopy imaging was performed to visually observe the uptake and permeation of SLNs through the intestinal wall. Figure 7B−D illustrates the confocal microscopy images of the intestinal cross sections treated with Rhodamine B loaded SLNs of abiraterone acetate; Figure 7B portrays the image of the intestine without z-stacking; and Figure 7C,D shows the images of the intestine under z-stacking at 5 and 10 μm depth, respectively. SLNs tagged with dye showed clear pictures of fluorescent particles permeated into the intestine which can be clearly observed from the fluorescent observed for the intact SLNs. The measurement of the depth of penetration of Rhodamine B tagged SLNs was performed by z-stacking showed penetration up to 10 μm. This might have been possible due to the nanometric size of the SLNs which were also intact in appearance during the uptake process via intestinal wall.[16,17,26] The study construed good *ex vivo* permeability of SLNs for the better systemic delivery and availability of the abiraterone acetate. The high permeability of SLNs was observed because of their nanometric size and highly lipophilic nature favoring transcellular and paracellular transport across the intestinal epithelial cell lining for availability in the systemic circulation.[13,16,26,34]

2.5.7. In Vivo Pharmacokinetic Studies. The pharmacokinetic profile of abiraterone acetate from different treatment formulations has been shown in Figure 8, which indicates significant augmentation in the absorption parameters ($p < 0.001$) of the drug from SLNs as compared to the free drug suspension.

The pharmacokinetic modeling of the obtained data showed good fitting with a one-compartment open body model with no lag-time of absorption, which was confirmed from higher values of the correlation coefficient, Akaike information criteria and Schwartz Bayesian criteria, as compared to that of the two-compartment body model. Table 3 enlists the pharmacokinetic

https://doi.org/10.1021/acsomega.1c07254
ACS Omega 2022, 7, 16968−16979

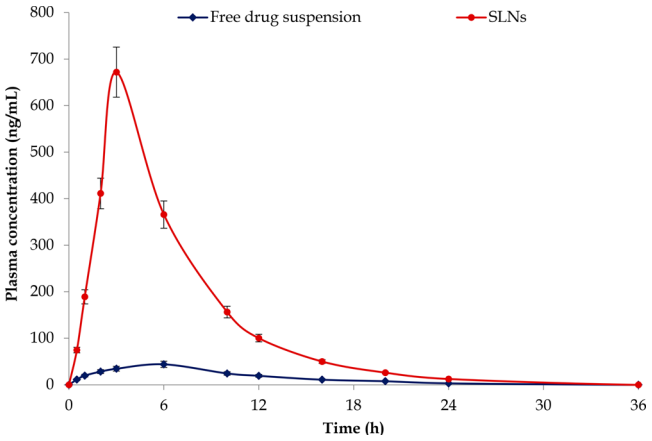

Figure 8. Pharmacokinetic profiles of abiraterone acetate from the free drug suspension and SLNs after oral administration Wistar rats; data expressed as mean ± SD (n = 6). Significant statistical difference (p < 0.001) observed between both the treatment groups at all the time points.

absorption parameters of abiraterone acetate from SLNs and free drug suspension. Very interestingly over 8.52-fold enhancement in $AUC_{0\text{-}t}$ and 15.24-folds improvement in C_{max} of the drug was observed from SLNs as compared to the free drug suspension of abiraterone acetate. Besides, T_{max} of the drug exhibited a 0.52-fold reduction from SLNs as compared to the free drug suspension, which indicated an increase in the rate of drug absorption from the SLN. Apart from these parameters, SLNs showed 0.72 to 0.81-fold improvement in MRT and K_a of the drug as compared to the free drug suspension. The enhanced drug absorption characteristics of the SLNs are quite obvious because of their lipidic nature which helped them in faster drug absorption through gastrointestinal epithelial cell lining.[13,17,26,32]

3. MATERIALS AND REAGENTS

Abiraterone acetate was provided by Glenmark Pharmaceuticals Limited, Mumbai, India. Compritol ATO 888, Precirol ATO 5, and Gelucire 50/13 were generously provided by Gattefosse India Pvt. Ltd. Mumbai, India. Glyceryl monostearate was purchased from Merck Limited, Mumbai, India, while Tween 80 and Poloxamer 407 were obtained from SD Fine Chemicals Ltd., Mumbai, India. Acetonitrile and methanol were purchased from Spectrochem Pvt. Ltd., Mumbai, India. Dialysis bag (mol. wt. cutoff 12 kDa), Dulbecco's modified eagle media (DMEM), penicillin-streptomycin medium, and Rhodamine B dye were purchased from Himedia Pvt. Ltd., Mumbai, India. PC-3 cells (grade IV prostate carcinoma) were obtained from National Centre for Cell Line, Pune, India.

4. EXPERIMENTAL METHODS

4.1. Analytical Method for Estimation of the Drug. The analytical estimation of the drug abiraterone acetate was carried out as per our previously developed and validated high-performance liquid chromatography (HPLC) method.[35] Waters Alliance e2695 HPLC system (Water Co, MA, U.S.A.) equipped with a separating module, autosampler, degasser, column oven, and photodiode array detector (Water 2996) was used for the analysis. The estimation was performed on a Hypersil BDS C_{18} column (250 × 4 mm; 5 μm; Thermo-Fisher, Tokyo, Japan) using 0.1% orthophosphoric acid in water (pH 3.5) and acetonitrile in the ratio of 15:85 as mobile phase and the flow rate was kept at 1 mL·min^{-1}. Other parameters like column temperature were kept at 25 °C, UV detection was performed at 250 nm and 10 μL injection volume was used. Data acquisition was performed using Empower version 2.0 software.

4.2. Selection of the Lipids. The solubility of abiraterone acetate was determined in various lipids. An excess amount of the drug was added to the vials containing 0.5 g of lipids and subjected to mechanical shaker for 24 h in a thermostatically controlled water bath shaker maintained at 85 ± 2 °C. The amount of drug solubilized in lipids was estimated by HPLC.

4.3. Selection of Surfactant and Cosurfactant. Surfactants and cosurfactants (S/Cos) selected were made on the basis of their emulsification capacity with lipids having maximal drug solubility. In brief, a binary mixture of S/Cos was prepared in equal ratios (1:1), mixed with lipid, and then titrated with water at different weight ratios from 1:9 to 9:1. The formation of primary microemulsion was taken as the end point and phase clarity was observed by measuring the transmittance of the diluted mixture at 510 nm with the help of UV−visible spectrophotometer (Shimadzu 3000+, Tokyo, Japan).

4.4. Preparation of the Abiraterone Acetate Loaded SLNs. The SLNs were prepared from the biomimetic lipids with maximal drug solubility by the modified emulsion/solvent evaporation method as described in the literature.[13,16] Initially, the organic phase was prepared by dissolving abiraterone acetate (10 mg), glyceryl monostearate (40 mg), and soya lecithin (10 mg) in ethanol (2 mL) under magnetic stirring at 100 rpm for 15 min to obtain a clear phase. The aqueous phase contained surfactant (Tween 80) and cosurfactant (Poloxamer 407) dissolved at 1% w/w concentration in 10 mL of double distilled water. The aqueous phase was then rapidly injected into the organic phase under continuous stirring conditions at 1500 rpm for 30 min which allowed complete evaporation of ethanol from the organic phase. The obtained dispersion containing SLNs was subjected to ultrasonication with a probe sonicator for 5 min. The SLNs were stored in glass vials in a cool dry place at ambient temperature conditions.

4.5. Preparation of the Rhodamine B Loaded Abiraterone Acetate SLNs. The abiraterone acetate SLNs

Table 3. Pharmacokinetic Parameters of Abiraterone Acetate Observed from SLNs and Free Drug Suspension in Wistar Rats

	pharmacokinetic parameters[a]					
treatments type[d]	c_{max} (ng/ml)[b]	$AUC_{0\text{-}t}$ (ng/mL/h)[b]	T_{max} (h)[b]	K_e (h^{-1})[c]	MRT (h)[c]	$T_{0.5}$ (h^{-1})[c]
free drug	44.11 ± 6.46	500.66 ± 8.76	6.56 ± 0.34	3.34 ± 1.01	7.33 ± 0.87	4.82 ± 1.72
SLNs	672.12 ± 7.21	4257.98 ± 10.29	3.35 ± 0.75	2.71 ± 0.98	6.88 ± 1.11	3.91 ± 0.98

[a]Data expressed as mean ± SD (n = 6). [b]Highly significant difference (p < 0.001). [c]Significant difference (p < 0.05). [d]Significant statistical difference in parameters of SLNs vis-à-vis free drug suspension.

https://doi.org/10.1021/acsomega.1c07254
ACS Omega 2022, 7, 16968−16979

loaded with Rhodamine B dye were prepared as per the same procedure described in Section 2.4. An aliquot of 1000 μL of Rhodamine B (0.05% w/v) solution was added to the aqueous phase during the preparation of SLNs. The unentrapped dye was removed from the SLNs with the help of the dialysis bag method where 2 mL dispersion of Rhodamine B loaded SLNs were washed in a dialysis bag for 3 h in phosphate buffer saline solution (pH 7.4).[36] The obtained product was lyophilized and stored in glass vials for further studies.

4.6. Preparation of the Abiraterone Acetate Suspension. The free drug suspension was prepared by dispersing 10 mg of abiraterone acetate in 10 mL of double distilled water containing 0.5% w/v sodium carboxymethylcellulose solution. The suspension was thoroughly stirred for attaining uniform dispersion of the drug.

4.7. Systematic Optimization of the SLNs Using Experimental Design. Box-Behnken design (BBD) was employed for response surface optimization of the SLNs. The concentration of glyceryl monostearate (mg), Tween 80 (%), and Poloxamer 407 (%) was taken as the highly influential factors for optimization of the SLNs, which were evaluated for the particle size (nm), polydispersity index, and entrapment efficiency (%) as the dependent variables. Design Expert software version 9.0.4.1 (Stat-Ease Inc., MN, U.S.A.) was used for applying BBD, where a total of 15 trial formulations of abiraterone acetate loaded SLNs were performed and evaluated for the responses. The mathematical model establishment, data analysis, and statistical validity measurement were performed. Model suitability was confirmed on the basis of *p*-value, correlation coefficient, and predicted error. The final step of selection of the optimized formulation was carried out by numerical search method to pass the desirability function. Also, the graphical search method was used for locating the chosen optimum formulation in the design space region of the overlay plot. Validation of the mathematical model was carried out by identifying check-point formulations to compare predicted and experimental values of the results, where a percent prediction error within ±5% was considered acceptable.

4.8. Characterization of the Abiraterone Acetate-Loaded SLNs. *4.8.1. Particle Size, Polydispersity Index, and Zeta Potential.* The particle size, polydispersity and zeta potential of SLNs were measured using Zetasizer (Nano ZS, Malvern Instrument, U.K.) at 25 °C. The zetasizer was equipped with a red laser of wavelength λ_0 = 633 nm (He−Ne, 4.0 MW).

4.8.2. Entrapment Efficiency (%). The entrapment efficiency (%) of the SLNs was determined by an indirect method where the amount of free drug present in the dispersion was quantified. One milliliter of the prepared drug-loaded SLN dispersion was centrifuged at 10 000 rpm for 30 min at 4 °C. The supernatant fraction was collected and suitably diluted with methanol for extraction of drug from the nanoparticles. The amount of free drug (unentrapped) in nanoparticles was quantified by HPLC.[35] Entrapment efficiency was calculated using the following eq 1

$$\text{Entrapment efficiency (\%)} = \frac{\text{Amount of drug taken} - \text{Amount of unentrapped drug}}{\text{Amount of drug taken}} \times 100 \quad (1)$$

4.8.3. Scanning Electron Microscopy (SEM). For SEM analysis, the freeze-dried nanoparticles were mounted on an aluminum stub, and gold−palladium alloy sputtering was performed to minimize the surface charge. Images were taken using a scanning electron microscope (Leo Electron Microscopy Ltd., Cambridge, U.K.) at 7.3 mm working distance and 5 kV accelerating voltage.

4.8.4. In Vitro Drug Release Study. The lyophilized SLNs dispersed in distilled water (1 mL) enclosed in dialysis bags (nitrocellulose membrane, mol. wt. 12 kDa) were subjected to release study by incubating with 25 mL of 0.1 N HCl (pH 1.2) and phosphate buffer solution (pH 6.8) containing 0.25% v/v sodium dodecyl sulfate at 100 rpm and 37 ± 2 °C under mild agitation in a water bath. At specified time intervals, 1 mL samples were withdrawn from the incubation medium and replaced with an equal volume of fresh medium. The drug content in the samples was analyzed by the HPLC method, and the control experiment was performed to obtain the release profile of the free drug suspension. The cumulative percent drug release was calculated using the below mentioned eq 2

$$\text{\%Drug release} = \frac{\text{Volume of release medium (ml)} \times \text{dilution factor} \times \text{peak area}}{\text{Intial amount of drug taken}} \times 100 \quad (2)$$

4.8.5. In Vitro Cell Culture Studies. The cell culture studies were performed on PC-3 cell line (human grade IV prostate carcinoma cells) which was purchased from National Centre for Cell Science, Pune, India. The cells received in lyophilized vials were grown in tissue culture flasks and kept in an incubator under controlled temperature of 37 °C and were supplied with 95% O_2/5% CO_2. The cells were regularly supplied with Dulbecco's Modified Eagle's medium, fetal bovine serum, penicillin and streptomycin medium for growth medium.

4.8.5.1. Cellular Cytotoxicity. The PC-3 cells (8×10^3 cells/well) were seeded in 96-well plates and incubated for 24 h for adherence to the wells. Subsequently, the cells were incubated with blank SLNs, drug-loaded SLNs and free drug suspension in the standard culture medium. After 72 h incubation, the cells were washed with phosphate buffer saline and incubated with 3-(4,5-dimethylthiazol-2-yl)-2,5-diphenyl tetrazolium bromide (MTT) dye for 4 h. The cells were again washed with phosphate buffer saline and incubated with dimethylsulfoxide to dissolve the formazan crystals. The absorbance of cells was measured at 570 nm against the untreated cells as control. The cell viability was expressed as the percentage absorbance of treatment groups with respect to the control. IC_{50} values (μg/mL) were calculated using SPSS software (IBM, Chicago).

4.8.5.2. Cellular Uptake. To investigate the cellular uptake of the nanoparticles, the cells were incubated with the drug-loaded SLNs tagged with Rhodamine B (in two groups) as well as the plain dye for 4 h. The cells were subjected to confocal laser scanning microscopy (CLSM, Leica TCS SP8, Wetzlar, Germany) to evaluate the fluorescence intensity for Rhodamine B at an excitation wavelength at 546 nm and an emission wavelength at 568 nm. Before mounting the slides onto a confocal microscope, the cells were washed five times with PBS for 1 min each.

4.9. Animal Experiments. All the animal experiments used in this work were subjected to prior approval from Institutional Animal Ethics Committee, Jamia Hamdard, New Delhi, India, under study protocol reference no. 1666). Male Wistar rats weighing between 180−250 g were used for the

https://doi.org/10.1021/acsomega.1c07254
ACS Omega 2022, 7, 16968−16979

study. Animals were housed in the central animal facility of the university and subjected to overnight fasting with free access to water prior to study initiation.

4.9.1. Ex Vivo Permeation and Confocal Imaging Studies. The small intestine was excised from the rats subjected to euthanasia by cervical dislocation. A small portion of the intestinal section (8−10 cm) was everted with the help of a glass rod and filled with test drug solution (typically 1.0 mL), while both the openings of the intestine were tied with the thread. Aliquot 200 μL Rhodamine B (0.05%) was added to 2 mL of the drug-loaded SLNs and stirred for 30 min for loading of the dye into the nanoparticles. Because of the photodegradation property of Rhodamine B, care and precautions were taken during the sample preparation. After this, 1 mL of prepared sample was added to the sac of freshly excised rat intestine and poured into the phosphate buffer solution (pH 6.5) as the media for diffusion. This cell was kept on a magnetic stirrer and allowed to stir at 300 rpm at 37 ± 0.5 °C, and the permeation study was performed for 6 h. At different time intervals, a 1 mL sample was withdrawn from the media and equal volume was replaced with fresh phosphate buffer solution to maintain sink conditions. The amount of drug permeated through the intestinal sac was estimated by HPLC analysis. After completion of the permeation experiment, the intestinal sac was collected and washed. Then, the sac was subjected to microtomy for preparing the slides for confocal laser scanning microscopy imaging under excitation and emission wavelengths Rhodamine B at 540 and 625 nm, respectively.

4.9.2. In Vivo Pharmacokinetic Studies. 4.9.2.1. Study Design and Blood-Sampling. A single-dose and randomized design was used for pharmacokinetic evaluation of the drug under the fasting conditions. The animals were orally administered with drug-loaded SLNs and free drug suspension, each containing 10 mg of abiraterone acetate. Blood samples were collected from animals under light anesthesia using a CO_2 chamber at specified time intervals of 0.5, 1, 3, 6, 12, 16, 18, 24, and 48 h. Plasma was separated by centrifugation at 10 000 rpm for 15 min and a fixed concentration of internal standard was added to the samples. Liquid−liquid extraction was used for the separation of the drug from rat plasma (50 μL) by adding t-butyl methyl ether (200 μL) in the ratio of 1:4, vortexed 5 min for thorough mixing and samples were centrifuged at 15 000 rpm for 30 min. The supernatant organic fraction was separated into a fresh eppendorf tube and evaporated under a nitrogen environment. The dried residue was then reconstituted with mobile phase and filtered through 0.22 μm membrane filter for estimation of abiraterone and internal standard in the rat plasma.

4.9.2.2. Sample Analysis by UPLC-MS/MS. The drug concentration in plasma was estimated using a validated bioanalytical UPLC-MS/MS method for quantification of abiraterone (active metabolite) and imatinib (internal standard), that is, ACQUITY UPLC-MS/MS system (Waters Inc., Milford, U.S.A.) fitted with Zspray Xevo TQD mass spectrometer. Chromatographic separation of the analyte and internal standard in rat plasma was performed on a C_{18} column (100 mm, 1.7 μm particle size), using ammonium acetate (2 mM) in water (pH 3.5) and acetonitrile with 0.1% formic acid as the mobile phase mixture. The isocratic elution was used for the mobile phase delivered at a flow rate of 0.4 mL/min, and run time was kept at 5 min. Linear calibration plot of the drug spiked in rat plasma was analyzed over the concentration ranging between 1 and 800 ng·mL^{-1}. The run time was kept at 5 min, while retention times for abiraterone and the internal standard were observed at 2.4 and 3.6 min, respectively. The detection was made by multiple reactions monitoring of parent-to-daughter ion transition at m/z 350.1 → 156.15 for abiraterone and m/z 494.43 → 294.17 for the internal standard. The plasma concentration data obtained at various time points were subjected to fitting with various compartmental body models and pharmacokinetic parameters (C_{max}, T_{max}, $AUC_{0\text{-}t}$, MRT, K_a and $t_{0.5}$) were calculated.

4.10. Statistical Data Analysis. The statistical analysis of data was performed by two-way ANOVA, followed by posthoc analysis by Dunnett's multiple comparisons test with 5% statistical significance.

5. CONCLUSIONS

The present research attempting to develop optimized SLNs revealed significant improvement in the oral bioavailability of the drug abiraterone acetate. The optimized SLNs revealed a particle size of 197.7 nm, polydispersity index of 0.26, zeta potential of 110.4 mV, and drug entrapment efficiency of 75%. The *in vitro* drug release performance evaluation indicated a sustained drug release nature of the SLNs with an increase in the extent of drug release during the entire period of a 24 h time course as compared to the pure drug suspension. *Ex vivo* permeation studies revealed a 3.75-times increase in the cumulative drug permeated from SLNs while *in vivo* studies indicated significant improvement (C_{max} and AUC) in the biopharmaceutical performance of the drug. Higher bioavailability observed from the SLNs also revealed multifold improvement in the anticancer activity by significant reduction (12.5-folds) of the IC_{50} value. To conclude, all of the studies determined that optimized SLNs showed enhanced oral bioavailability and anticancer activity of the drug for the management of prostate carcinoma.

■ ASSOCIATED CONTENT

Supporting Information

The Supporting Information is available free of charge at https://pubs.acs.org/doi/10.1021/acsomega.1c07254.

(Table S1) ANOVA results for response surface quadratic model for particle size; (Table S2) ANOVA results for response surface quadratic model for PDI; (Table S3) ANOVA results for response surface quadratic model for entrapment efficiency; (Table S4) comparison of predicted and experimental values of the responses of optimized SLNs and check-point formulations (PDF)

■ AUTHOR INFORMATION

Corresponding Authors

Sarwar Beg − *Department of Pharmaceutics, School of Pharmaceutical Education and Research, Nanomedicine Research Lab, Jamia Hamdard, New Delhi 110062, India;* orcid.org/0000-0002-3304-2712; Email: sarwar.beg@jamiahamdard.ac.in, sarwar.beg@gmail.com

Mohammad Javed Ansari − *Department of Pharmaceutics, College of Pharmacy, Prince Sattam Bin Abdulaziz University, Al-kharj 16278, Saudi Arabia;* Email: ankitmalik292@gmail.com

https://doi.org/10.1021/acsomega.1c07254
ACS Omega 2022, 7, 16968−16979

Authors

Ankit K. Malik − *Department of Pharmaceutics, School of Pharmaceutical Education and Research, Nanomedicine Research Lab, Jamia Hamdard, New Delhi 110062, India*

Asrar A. Malik − *School of Basic Sciences and Research, Department of Life Sciences, Sharda University, Greater Noida, Uttar Pradesh 201306, India*

Ahmed Mahmoud Abdelhaleem Ali − *Department of Pharmaceutics and Industrial Pharmacy, College of Pharmacy, Taif University, Taif 21944, Saudi Arabia;* orcid.org/0000-0002-4370-007X

Abdulrahman Theyab − *Department of Laboratory Medicine, Security Forces Hospital, Mecca 21955, Saudi Arabia*

Mohammad Algahtani − *Department of Laboratory Medicine, Security Forces Hospital, Mecca 21955, Saudi Arabia*

Waleed H. Almalki − *Department of Pharmacology and Toxicology, College of Pharmacy, Umm Al-Qura University, Al-Abidiyah 21955, Saudi Arabia*

Khalid S. Alharbi − *Department of Pharmacology, College of Pharmacy, Jouf University, Sakakah 72388, Saudi Arabia*

Sattam K. Alenezi − *Department of Pharmacology and Toxicology, Unaizah College of Pharmacy, Qassim University, Qassim 52222, Saudi Arabia*

Md. Abul Barkat − *Department of Pharmaceutics, College of Pharmacy, University of Hafr, Al Batin 39524, Saudi Arabia*

Mahfoozur Rahman − *Department of Pharmaceutical Sciences, Shalom Institute of Health and Allied Sciences, Sam Higginbottom University of Agriculture, Technology and Sciences, Allahabad 211007, India*

Hani Choudhry − *Department of Biochemistry, Cancer Metabolism and Epigenetic Unit, Faculty of Science, King Fahd Center for Medical Research, King Abdulaziz University, Jeddah 21589, Saudi Arabia*

Complete contact information is available at: https://pubs.acs.org/10.1021/acsomega.1c07254

Author Contributions

■S.B. and A.K.M. have equal contribution in the present work.

Notes

The authors declare no competing financial interest.

■ ACKNOWLEDGMENTS

The authors of this research would like to acknowledge the financial support offered by Taif University Researchers Supporting Project Number TURSP-2020/50, Taif University, Saudi Arabia.

■ REFERENCES

(1) Sung, H.; Ferlay, J.; Siegel, R. L.; Laversanne, M.; Soerjomataram, I.; Jemal, A.; Bray, F. Global Cancer Statistics 2020: GLOBOCAN Estimates of Incidence and Mortality Worldwide for 36 Cancers in 185 Countries. *CA: Cancer J. Clin.* **2021**, *71*, 209−249.

(2) He, L.; Fang, H.; Chen, C.; Wu, Y.; Wang, Y.; Ge, H.; Wang, L.; Wan, Y.; He, H. Metastatic castration-resistant prostate cancer: Academic insights and perspectives through bibliometric analysis. *Medicine* **2020**, *99*, No. e19760.

(3) Saad, F.; Bogemann, M.; Suzuki, K.; Shore, N. Treatment of nonmetastatic castration-resistant prostate cancer: focus on second-generation androgen receptor inhibitors. *Prostate Cancer Prostatic Dis.* **2021**, *24*, 323−334.

(4) Nuhn, P.; De Bono, J. S.; Fizazi, K.; Freedland, S. J.; Grilli, M.; Kantoff, P. W.; Sonpavde, G.; Sternberg, C. N.; Yegnasubramanian, S.; Antonarakis, E. S. Update on systemic prostate cancer therapies: Management of metastatic castration-resistant prostate cancer in the era of precision oncology. *Eur. Urol.* **2019**, *75*, 88−99.

(5) Pal, S. K.; Lewis, B.; Sartor, O. Management of docetaxel failures in metastatic castrate-resistant prostate cancer. *Urologic Clin. North Am.* **2012**, *39*, 583−591.

(6) Akaza, H.; Procopio, G.; Pripatnanont, C.; Facchini, G.; Fava, S.; Wheatley, D.; Leung, K. C.; Butt, M.; Silva, A.; Castillo, L.; et al. Metastatic Castration-Resistant Prostate Cancer Previously Treated With Docetaxel-Based Chemotherapy: Treatment Patterns From the PROXIMA Prospective Registry. *J. Global Oncol.* **2018**, *4*, 1−12.

(7) Kluetz, P. G.; Ning, Y.-M.; Maher, V. E.; Zhang, L.; Tang, S.; Ghosh, D.; Aziz, R.; Palmby, T.; Pfuma, E.; Zirkelbach, J. F.; et al. Abiraterone Acetate in Combination with Prednisone for the Treatment of Patients with Metastatic Castration-Resistant Prostate Cancer: U.S. Food and Drug Administration Drug Approval Summary. *Clin. Cancer Res.* **2013**, *19*, 6650.

(8) Stuyckens, K.; Saad, F.; Xu, S.; Ryan, C. J.; Smith, M. R.; Griffin, T. W.; Yu, M. K.; Vermeulen, A.; Nandy, P.; Poggesi, I. Population pharmacokinetic analysis of abiraterone acetate in healthy volunteers and chemotherapy-naive and chemotherapy-pretreated metastatic castration-resistant prostate cancer patients. *J. Clin. Oncol.* **2014**, *32*, 58−58.

(9) Chi, K. N.; Spratlin, J.; Kollmannsberger, C.; North, S.; Pankras, C.; Gonzalez, M.; Bernard, A.; Stieltjes, H.; Peng, L.; Jiao, J.; et al. Food effects on abiraterone pharmacokinetics in healthy subjects and patients with metastatic castration-resistant prostate cancer. *J. Clin. Pharmacol.* **2015**, *55*, 1406−1414.

(10) Payne, H.; Bahl, A.; Mason, M.; Troup, J.; De Bono, J. Optimizing the care of patients with advanced prostate cancer in the UK: current challenges and future opportunities. *BJU Int.* **2012**, *110*, 658−667.

(11) Basa-Denes, O.; Solymosi, T.; Otvos, Z.; Angi, R.; Ujhelyi, A.; Jordan, T.; Heltovics, G.; Glavinas, H. Investigations of the mechanism behind the rapid absorption of nano-amorphous abiraterone acetate. *Eur. J. Pharm. Sci.* **2019**, *129*, 79−86.

(12) Gala, U.; Miller, D.; Williams, R. O., 3rd Improved dissolution and pharmacokinetics of abiraterone through KinetiSol enabled amorphous solid dispersions. *Pharmaceutics* **2020**, *12*, 357.

(13) Beg, S.; Jain, S.; Kushwah, V.; Bhatti, G. K.; Sandhu, P. S.; Katare, O. P.; Singh, B. Novel surface-engineered solid lipid nanoparticles of rosuvastatin calcium for low-density lipoprotein-receptor targeting: a Quality by Design-driven perspective. *Nanomedicine* **2017**, *12*, 333−356.

(14) Swain, S.; Sahu, P. K.; Beg, S.; Babu, S. M. Nanoparticles for cancer targeting: Current and future directions. *Curr. Drug Delivery* **2016**, *13*, 1290−1302.

(15) Harshita; Barkat, M. A.; Das, S. S.; Pottoo, F. H.; Beg, S.; Rahman, Z. Lipid-Based Nanosystem As Intelligent Carriers for Versatile Drug Delivery Applications. *Curr. Pharm. Des.* **2020**, *26*, 1167−1180.

(16) Beg, S.; Choudhry, H.; Zamzami, M. A.; Alharbi, K. S.; Rahman, M.; Singh, B. Nanocolloidal lipidic carriers of olmesartan medoxomil surface-tailored with Concavalin-A for lectin receptor targeting. *Nanomedicine* **2018**, *13*, 3107−3128.

(17) Poonia, N.; Lather, V.; Narang, J. K.; Beg, S.; Pandita, D. Resveratrol-loaded folate targeted lipoprotein-mimetic nanoparticles with improved cytotoxicity, antioxidant activity and pharmacokinetic profile. *Mater. Sci. Eng., C* **2020**, *114*, 111016.

(18) Beg, S.; Barkat, M. A.; Ahmad, F. J. Advancement in Polymer and Lipid-based Nanotherapeutics for Cancer Drug Targeting. *Curr. Pharm. Des.* **2020**, *26*, 1127−1127.

(19) Harshita; Barkat, M. A.; Das, S. S.; Pottoo, F. H.; Beg, S.; Rahman, Z. Lipid-based nanosystem as intelligent carriers for versatile drug delivery applications. *Curr. Pharm. Des.* **2020**, *26*, 1167−1180.

(20) Singh, B.; Beg, S.; Raza, K. Developing "Optimized" Drug Products Employing "Designed" Experiments. *Chem. Ind. Digest* **2013**, *23*, 70−76.

(21) Beg, S.; Akhter, S.; Rahman, M.; Rahman, Z. Perspectives of quality by design approach in nanomedicines development. *Curr. Nanomed.* **2017**, *7*, 191−197.
(22) Beg, S.; Hasnain, M. S.; Rahman, M.; Swain, S. Chapter 1 - Introduction to Quality by Design (QbD): Fundamentals, Principles, and Applications. In *Pharmaceutical Quality by Design*; Academic Press: New York, 2019; pp 1−17.
(23) Beg, S.; Rahman, M.; Kawish, S. M.; Qadir, A.; Taleuzzaman, M.; Ilyas, R.; Alam, K.; Shukla, R.; Choudhry, H.; Souto, E. B.; et al. Quality by Design approach for systematic development of nano-formulations. In *Nanoformulation Strategies for Cancer Treatment*; Elsevier Inc.: New York, 2021; Chapter 20, pp 353−364.
(24) Beg, S.; Rahman, M.; Panda, S. S. Pharmaceutical QbD: Omnipresence in the product development lifecycle. *Eur. Pharm. Rev.* **2017**, *22*, 58−64.
(25) Beg, S.; Robaian, M. A.; Rahman, M.; Imam, S. S.; Alruwaili, N.; Panda, S. K. *Pharmaceutical drug product development and process optimization: Effective use of Quality by Design*; CRC Press: New York, 2020.
(26) Rahman, M.; Almalki, W. H.; Afzal, O.; Alfawaz Altamimi, A. S.; Kazmi, I.; Al-Abbasi, F. A.; Choudhry, H.; Alenezi, S. K.; Barkat, M. A.; Beg, S.; et al. Cationic solid lipid nanoparticles of resveratrol for hepatocellular carcinoma treatment: Systematic optimization, *in vitro* characterization and preclinical investigation. *Int. J. Nanomed.* **2020**, *15*, 9283−9299.
(27) Ellenberger, D. J.; Miller, D. A.; Williams, R. O. Expanding the application and formulation space of amorphous solid dispersions with KinetiSol: A review. *AAPS PharmSciTech* **2018**, *19*, 1933−1956.
(28) Rasmussen, M. K.; Pedersen, J. N.; Marie, R. Size and surface charge characterization of nanoparticles with a salt gradient. *Nature Comm.* **2020**, *11*, 2337−2345.
(29) Masood, S. A.; Maheen, S.; Khan, H. U.; Zafar, M. N.; Shafqat, S. S.; Mujtaba, M. A.; ur Rehman, A.; Abbas, G.; Mahmood, M. H. R.; Bashir, S.; et al. In vitro/in vivo evaluation of statistically engineered alginate scaffold reinforced with dual drugs loaded silica nanoparticles for enhanced fungal therapeutics. *Alexandria Eng. J.* **2022**, *61*, 4041−4056.
(30) Masood, A.; Maheen, S.; Khan, H. U.; Shafqat, S. S.; Irshad, M.; Aslam, I.; Rasul, A.; Bashir, S.; Zafar, M. N. Pharmaco-technical evaluation of statistically formulated and optimized dual drug-loaded silica nanoparticles for improved antifungal efficacy and wound healing. *ACS Omega* **2021**, *6*, 8210−8225.
(31) Wang, L.; Wang, X.; Shen, L.; Alrobaian, M.; Panda, S. K.; Almasmoum, H. A.; Ghaith, M. M.; Almaimani, R. A.; Ibrahim, I. A. A.; Singh, T.; et al. Paclitaxel and naringenin-loaded solid lipid nanoparticles surface modified with cyclic peptides with improved tumor targeting ability in glioblastoma multiforme. *Biomed. Pharmacother.* **2021**, *138*, 111461.
(32) Schultz, H. B.; Meola, T. R.; Thomas, N.; Prestidge, C. A. Oral formulation strategies to improve the bioavailability and mitigate the food effect of abiraterone acetate. *Int. J. Pharm.* **2020**, *577*, 119069.
(33) Schultz, H. B.; Wignall, A. D.; Thomas, N.; Prestidge, C. A. Enhancement of abiraterone acetate oral bioavailability by super-saturated-silica lipid hybrids. *Int. J. Pharm.* **2020**, *582*, 119264.
(34) Pandey, P.; Rahman, M.; Bhatt, P. C.; Beg, S.; Paul, B.; Hafeez, A.; Al-Abbasi, F. A.; Nadeem, M. S.; Baothman, O.; Anwar, F.; et al. Implication of nano-antioxidant therapy for treatment of hepatocellular carcinoma using PLGA nanoparticles of rutin. *Nanomedicine* **2018**, *13*, 849−870.
(35) Beg, S.; Malik, A. K.; Afzal, O.; Altamimi, A. S. A.; Kazmi, I.; Al-Abbasi, F. A.; Almalki, W. H.; Barkat, M. A.; Kawish, S. M.; Pradhan, D. P.; et al. Systematic development and validation of a RP-HPLC method for estimation of abiraterone acetate and its degradation products. *J. Chromatograph. Sci.* **2021**, *59*, 79−87.
(36) Parvez, S.; Yadagiri, G.; Gedda, M. R.; Singh, A.; Singh, O. P.; Verma, A.; Sundar, S.; Mudavath, S. L. Modified solid lipid nanoparticles encapsulated with Amphotericin B and Paromomycin: An effective oral combination against experimental murine visceral leishmaniasis. *Sci. Rep.* **2020**, *10*, 12243.

https://doi.org/10.1021/acsomega.1c07254
ACS Omega 2022, 7, 16968−16979